

# Relationship Between Occurrence of Neurological Disorders and Coronavirus Infection via Protein-Protein Sequence Matching Analysis Technique and Repurposing Neuroprotective Agents in the Treatment of Coronavirus Infection

Prinsa <sup>1,\*</sup> , Supriyo Saha <sup>2,\*</sup> 

<sup>1</sup> Department of Pharmaceutical Chemistry, Siddhartha Institute of Pharmacy, Sahastradhara Near IT Park, Dehradun, Uttarakhand, India.; [prinsapharmacist@gmail.com](mailto:prinsapharmacist@gmail.com);

<sup>2</sup> Department of Pharmaceutical Chemistry, Uttaranchal Institute of Pharmaceutical Sciences, Uttaranchal University, Dehradun, Uttarakhand, India.; [supriyo9@gmail.com](mailto:supriyo9@gmail.com);

\* Correspondence: [prinsapharmacist@gmail.com](mailto:prinsapharmacist@gmail.com) (P), [supriyo9@gmail.com](mailto:supriyo9@gmail.com) (S.S)

Scopus Author ID: 55844991200

Received: 18.10.2023; Accepted: 12.05.2024; Published: 21.09.2024

**Abstract:** Nowadays, one out of three coronavirus patients are infected with any form of neurological disorder like Alzheimer's, Parkinson's, multiple sclerosis, and dementia. There is no proper explanation behind the occurrence of neurological disorders during COVID-19 infection. To establish a relationship between coronavirus (wild type and mutant strains) and neurological disorders and identify the best neuroprotective agent to conquer both coronavirus infection and neurological disorder(s). Here, we performed protein-protein sequence similarity analysis between the FASTA sequence belonging to coronavirus (wild type and mutant strains) and the FASTA sequence of receptors belonging to neurological disorders. Also performed molecular docking studies between coronavirus (wild type and mutant strains) receptors 6LU7, 7NEH, and twenty-five neuroprotective agents. These sequence similarity data revealed that if a patient suffered from any coronavirus infection (wild type or mutant), there was a chance for the occurrence of neurological disorders associated with PCSK9 fab 6E2 lead brain injury, and connective tissue insulation, tau protein accumulation related Alzheimer as well as abnormal dopaminergic D2 receptor linked Parkinson disease. The molecular docking studies data showed that among all the neuroprotective agents that showed good receptor-ligand interaction, bromoergocryptine was observed with the best interaction with both the receptors (6LU7 and 7NEH) as well as fitted with receptor active site. So, if we consider bromoergocryptine in treating coronavirus infection, it may act as a good remedy for "Therapy of COVID-19" without any neurological disorder.

**Keywords:** Coronavirus; neurological disorders; FASTA sequence similarity; neuroprotective agents, molecular docking studies.

© 2024 by the authors. This article is an open-access article distributed under the terms and conditions of the Creative Commons Attribution (CC BY) license (<https://creativecommons.org/licenses/by/4.0/>).

## 1. Introduction

We are in half past 2023 but still struggling with the pandemic situation caused by COVID-19. Different types of proteins are observed in coronavirus, such as replicase polyprotein, spike glycoprotein, ORF9b, and 2'-O-methyltransferase [1]. This virus is expressed in various organisms before infecting humans, such as feline, murine, bat, bovine, avian, porcine, rat, etc [2]. Till now, a total of 163,250,829 persons have been infected, with

almost 3,385,473 deaths reported and still counting [3]. When a person gets infected with coronavirus, his/her lungs are affected, and some serious neurological manifestations also occur in the veil. After being infected with the coronavirus, a person starts suffering from various neurological disorders like Alzheimer's, Parkinson's, multiple sclerosis, and dementia disease. In this context, a literature survey related to various data collection and analysis shows that one out of three patients suffering from coronavirus is concurrently infected with any of the above neurological disorders [4]. But it is our misfortune that, to date, we have not got any proper explanation (s) between coronavirus and neurological disorders relationship. A question automatically arises: Why does a viral protein (related to respiratory system infection) negatively affect neuronal regulation? [5] The virus was readily mutated from one variant to another. Among them, we selected the B 1.1.7 UK variant for our study [6,7]. Towards the establishment of a relationship between coronavirus and the occurrence of neurological disorders [8], we performed protein-protein BLAST between the FASTA sequence belonging to coronavirus (wild type and mutant strains) and the FASTA sequence of receptors belonging to neurological disorders [9]. Then, we also performed molecular docking interaction studies between selective neuroprotective agents and coronavirus receptors to identify the best neuroprotective agent to conquer both coronavirus infection and neurological disorder(s).

## 2. Materials and Methods

### 2.1. Selection of receptors.

#### 2.1.1. 6LU7.

6LU7 is the crystal structure of COVID-19 main protease in complex with an inhibitor N3. Researchers isolated the receptor from the synthetic form of severe acute respiratory syndrome coronavirus 2 with E. coli BL21 as an expression system. The receptor belongs to the 3C-proteinase family with 306 amino acids in chain length A. As per drug discovery studio, the surrounding residues of 6LU7 were THR 190, GLU 166, GLN 189, ASP 187, HIS 164, PHE 140, CYS 145, GLY 143, HIS 172, SER 144, ASN 142, LEU 141, HIS 163, GLN 192 and MET 165 [10].

#### 2.1.2. 7NEH.

The receptor belongs to the crystal structure of the receptor binding domain of SARS-CoV-2 Spike glycoprotein in complex with COVOX-269 Fab.

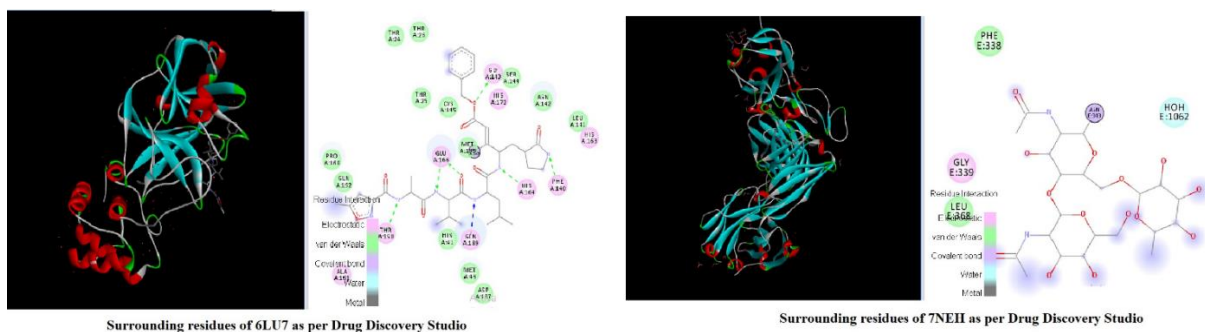


**Figure 1.** Active site residues of 6LU7 and 7NEH.

The receptor belongs to the immune system, isolated from *Homo sapiens* with the same expression system (Figure 1). It consists of three chains: the COVOX-269 fab heavy chain with 222 amino acids, the COVOX-269 fab light chain with 215 amino acids, and spike glycoprotein with amino acids with 205 amino acids. As per Drug Discovery Studio, the surrounding residues of 7NEH were ARG 346, THR 345, ARG 355, LYS 356 2.2 Å, GLU 340, SER 399, VAL 341, ALA 397, PHE 464 and ASN 354 [11].

#### 2.1.3. 1GOS.

1GOS is the crystal structure of human monooxidase amine B complexed with flavin adenine dinucleotide. Researchers procured the receptor from *Homo sapiens* with *Komagataella pastoris* as an expression system. The receptor consists of two chains with 520 amino acids on each chain.

#### 2.1.4. 2XFU.

2XFU is the crystal structure of human monooxidase amine B complexed with tranylcypromine. Researchers procured the receptor from *Homo sapiens* with *Komagataella pastoris* as an expression system. The receptor consists of two chains with 519 amino acids on each chain.

#### 2.1.5. 2BK3.

2BK3 is the crystal structure of human monooxidase amine B complexed with farnesol. Researchers procured the receptor from *Homo sapiens* with *Komagataella pastoris* as an expression system. The receptor consists of two chains with 520 amino acids on each chain [12].

#### 2.1.6. 1OJA.

1OJA is the crystal structure of human monooxidase amine B complexed with isatin. Researchers procured the receptor from *Homo sapiens* with *Komagataella pastoris* as an expression system. The receptor consists of two chains with 520 amino acids on each chain [13].

#### 2.1.7. 2BYB.

2BYB is the crystal structure of human monooxidase amine B complexed with deprenyl. Researchers procured the receptor from *Homo sapiens* with *Komagataella pastoris* as an expression system. The receptor consists of two chains with 520 amino acids on each chain [14].

#### 2.1.8. 3PO7.

3PO7 is the crystal structure of human monooxidase amine B complexed with zonisamide. Researchers procured the receptor from *Homo sapiens* with *Komagataella pastoris* as an expression system. The receptor consists of two chains with 520 amino acids on each chain.

2.1.9. 1OJD.

1OJD is the crystal structure of human mono oxidase amine B complexed with lauryl dimethylamine-N-oxide. Researchers procured the receptor from *Homo sapiens* with *Komagataella pastoris* as an expression system. The receptor consists of eight chains with 520 amino acids on each chain [15].

2.1.10. 4GRB.

4GRB is the crystal structure of casein kinase-2 complexed with 5-(2-{{4-(dimethylcarbamoyl)phenyl}amino}-4-methoxypyrimidin-5-yl)thiophene-3-carboxylic acid. Researchers procured the receptor from *Homo sapiens* with *Escherichia coli* as an expression system. The receptor consists of one chain with 333 amino acids [16].

2.1.11. 3U4U.

3U4U is the crystal structure of casein kinase-2 complexed with 3-{{5-(acetylamino)-3-[[3-cyano-7-(cyclopropylamino)pyrazolo[1,5-a]pyrimidin-5-yl]-1H-indol-1-yl]}propanoic acid. Researchers procured the receptor from *Homo sapiens* with *Escherichia coli* as an expression system. The receptor consists of one chain with 333 amino acids.

2.1.12. 5B3J.

5B3J is the crystal structure of N-methyl-D-aspartate receptors complexed with ifenprodil. Researchers procured the receptor from *Xenopus laevis*, *Rattus norvegicus*, and *Mus musculus* with *Trichoplusia ni* as an expression system. The receptor consists of two chains with 383 amino acids on each chain [17].

2.1.13. 5H8N.

5H8N is the crystal structure of glutamate and N-methyl-D-aspartate receptors complexed with 4-[[{4-fluorophenyl)sulfonylamino}methyl]-~{N}-(pyridin-3-ylmethyl)benzamide. Researchers procured the receptor from *Homo sapiens* with *Escherichia coli* as an expression system. The receptor consists of one chain with 285 amino acids.

2.1.14. 5H8Q.

5H8Q is the crystal structure of glutamate and N-methyl-D-aspartate receptors complexed with 6-[[ethyl-(4-fluorophenyl)amino]methyl]-2,3-dihydro-1~{H}-cyclopenta[3,4][1,3]thiazolo[1,4~{a}]pyrimidin-8-one. Researchers procured the receptor from *Homo sapiens* with *Escherichia coli* as expression system. The receptor consists of two chains; among them, the A chain consists of 285 amino acids, and the B chain consists of 293 amino acids.

2.1.15. 5H8S.

5H8S is the crystal structure of glutamate and N-methyl-D-aspartate receptors complexed with 7-[[ethyl(phenyl)amino]methyl]-2-methyl-[1,3,4]thiadiazolo[3,2-a]pyrimidin-5-one. Researchers procured the receptor from *Homo sapiens* with *Escherichia coli* as an expression system. The receptor consists of three chains with 263 amino acids on each chain [18].

2.1.16. 5IDE.

5IDE is the crystal structure of AMPA-type glutamate receptors. Researchers procured the receptor from *Rattus norvegicus* with *Homo sapiens* as an expression system. The receptor consists of four chains; chains A and C consist of 872 amino acids, and chains B and D with 874 amino acids [19].

2.1.17. 3DP4.

3DP4 is the crystal structure of AMPA-type glutamate receptors complexed with (S)-Alpha-Amino-3-hydroxy-5-methyl-4-isoxazolepropionic acid. Researchers procured the receptor from *Rattus norvegicus* with *Escherichia coli* as an expression system. The receptor consists of one chain with 278 amino acids.

2.1.18. 5VOV.

5VOV is the crystal structure of AMPA receptors coassembled with transmembrane AMPA receptor regulatory proteins. Researchers procured the receptor from *Rattus norvegicus* with *Homo sapiens* as an expression system. The receptor consists of four chains with 889 amino acids on each chain [20].

2.1.19. 5L1B.

5L1B is the crystal structure of AMPA subtype ionotropic glutamate receptor. Researchers procured the receptor from *Rattus norvegicus* with *Homo sapiens* as an expression system. The receptor consists of four chains with 803 amino acids on each chain.

2.1.20. 1BX4.

1BX4 is the crystal structure of the human adenosine kinase receptor. Researchers procured the receptor from *Homo sapiens* with *Escherichia coli* as an expression system. The receptor consists of one chain with 345 amino acids [21].

2.1.21. 6TCA.

6TCA is the crystal structure of Phosphorylated p38 and MAPKAPK2 receptor complexed with L-peptide. Researchers procured the receptor from *Homo sapiens* with *Escherichia coli* as an expression system. The receptor consists of four chains with 371 amino acids on each chain [22].

2.1.22. 6UNA.

6UNA is the crystal structure of the mitogen-activated protein p38 gamma kinase receptor. Researchers procured the receptor from *Homo sapiens* with *Escherichia coli* as an expression system. The receptor consists of two chains with 361 amino acids on each chain [23].

2.1.23. 4ACC.

4ACC is a GSK-3 $\beta$  enzyme receptor complexed with 3-amino-6-(4-([2-(dimethylamino)ethyl]sulfamoyl)phenyl)-n-pyridin-3-ylpyrazine-2-carboxamide (7YG) as a

ligand and dimethylsulfoxide. The researcher isolated the receptor from *Homo sapiens* with the *Trichoplusia ni* expressing system. Two chains of the receptor comprised 385 amino acids in both chains, with 266 molecules of water in chain A and 244 molecules of water in chain B.

#### 2.1.24. 4ACH.

4ACH is a GSK-3 $\beta$  enzyme receptor complexed with 3-amino-n-(3-methoxy propyl)-6-{4-[(4-methyl piperazine-1-yl)sulfonyl]phenyl}pyrazine-2-carboxamide (KDI) as a ligand. Scientists isolated the receptor from *Homo sapiens* with *Tri-choplusia ni* as an expressing system. It had two chains with 465 amino acids [24].

#### 2.1.25. 1UV5.

1UV5 is a GSK-3 $\beta$  enzyme receptor complexed with 6-bromoindirubin-3'-oxime (BRW) as a ligand. Researchers screened the receptor from *Homo sapiens* with *Spodoptera frugiperda* as an expression system [25].

#### 2.1.26. 6H0U.

6H0U is a GSK-3 $\beta$  enzyme receptor complexed with (2{R})-3-[7-azanyl-5-(cyclohexylamino)-[1,2,4]triazolo[1,5-a][1,3,5]triazin-2-yl]-2-cyano-propanamide (FKB) as ligand. Researchers screened the receptor from *Homo sapiens* with *Trichoplusia ni* as an expression system. It has two chains of 420 amino acids [26].

#### 2.1.27. 2V17.

2V17 is a structure of the complex of antibody MN423 with a fragment of tau protein. Researchers screened the receptor from *Homo sapiens* and *Mus musculus*. It has two chains with 222 and 214 amino acids.

#### 2.1.28. 6DCA.

6DCA is a structure Fab/epitope complex of mouse monoclonal antibody 6B2 targeting a non-phosphorylated tau epitope. Researchers screened the receptor from *Homo sapiens* and *Mus musculus*. It has four chains with 218 amino acids on each chain [27].

#### 2.1.29. 6DCW.

6DCW is the crystal structure of the human anti-tau antibody CBTAU-27.1 Fab in complex with a human tau peptide. Researchers screened the receptor from *Homo sapiens*. It has two chains with 220 and 231 amino acids [28].

#### 2.1.30. 5E2U.

5E2U is the crystal structure of anti-TAU AT8 FAB in the presence of phosphopeptide. Researchers screened the receptor from *Mus musculus* with *Homo sapiens* as an expression system. It has two chains with 219 and 222 amino acids [29].

2.1.31. 6E4Y.

6E4Y is the crystal structure of Anti-PCSK9 fab 6E2 bound to the N-terminal peptide from PCSK9. Researchers screened the receptor from *Mus musculus* and *Homo sapiens* with *Escherichia coli* as an expression system. It has two chains with 224 and 219 amino acids [30].

2.1.32. 6VMS.

6VMS is the crystal structure of a D2 dopamine receptor-G-protein complex in a lipid membrane with bromoergocryptine as a ligand. Researchers screened the receptor from *Rattus norvegicus*, *Homo sapiens*, and *Escherichia virus T4* with *Spodoptera frugiperda* as the expression system. It has five chains [31].

2.1.33. 1SOA.

1SOA is the crystal structure of human DJ-1 with sulfinic acid. Researchers screened the receptor from *Homo sapiens* with *Escherichia coli* BL21(DE3) as an expression system. It has one chain with 185 amino acids.

2.1.34. 4E08.

4E08 is the crystal structure of *Drosophila melanogaster* DJ-1beta. Researchers screened the receptor from *Drosophila melanogaster* with *Escherichia coli* BL21(DE3) as an expression system. It has two chains with 190 amino acids on each chain [32].

2.1.35. 6AFL.

6AFL is the crystal structure of DJ-1 with 5-fluoranyl-1-(2-phenylethyl)indole-2,3-dione as ligand. Researchers screened the receptor from *Homo sapiens* with *Escherichia coli* BL21(DE3) as an expression system. It has one chain with 189 amino acids.

2.1.36. 6U9W.

6U9W is the cryo electron microscopy structure of the ATP-gated rat P2X purinoceptor7 ion channel with O-[(R)-[(2S)-2-(hexadecanoyloxy)-3-(octadecanoyloxy)propoxy](hydroxy)phosphoryl]-D-serine as ligand. Researchers screened the receptor from *Rattus norvegicus* with *Homo sapiens* as an expression system. It has three chains with 609 amino acids on each chain.

2.1.37. 6U9V.

6U9V is the cryo electron microscopy structure of the ATP-gated rat P2X purinoceptor7 ion channel with O-[(R)-[(2S)-2-(hexadecanoyloxy)-3-(octadecanoyloxy)propoxy](hydroxy)phosphoryl]-D-serine as ligand. Researchers screened the receptor from *Rattus norvegicus* with *Homo sapiens* as an expression system. It has three chains with 609 amino acids on each chain [33].

2.2. *Performing protein-protein BLAST in search of similarity.*

In this context, we thoroughly searched various proteins/receptors associated with various neurological disorders. In this investigation, 6LU7 and 7NEH were considered as the

principal receptors belonging to wild-type and mutant (B.1.1.7) strains of coronavirus. Here, (1GOS, 2XFU,2BK3, 1OJA, 2BYB, 3PO7, 1OJD), (4GRB, 3U4U), (5B3J, 5H8N, 5H8Q, 5H8S), (5IDE, 3DP4, 5VOV, 5L1B), (1BX4), (6TCA, 6UNA), (4ACC, 4ACH, 1UV5,6H0U), (2V17, 6DCA, 6DCW, 5E2U,6E4Y), (6VMS, 1SOA, 4E08, 6AFL) and (6U9W, 6U9V) were considered for monoamine oxidase, casein kinase-2, N-methyl-D-aspartate,  $\alpha$ -amino-3-hydroxy-5-methyl-4-isoxazolepropionic acid, adenosine kinase, mitogen-activated protein kinase, glycogen synthase kinase, Tau protein, Tau/Fab and P2X purinoceptor-7 respectively towards neurological disorder related proteins/receptors category. Then, protein-protein BLAST (Basic Local Alignment Search Tool) was performed between FASTA sequence 6LU7, 7NEH, and the abovementioned neurological proteins/receptors [34].

### *2.3. Molecular docking studies between anti-alzheimer's drugs/anti-Parkinson drugs/neuroprotective agents with 6LU7 and 7NEH.*

#### *2.3.1. Selection of ligands.*

Here, we selected twenty-five ligands, i.e., baicalein, baicalein quinone, cinnamaldehyde, crystal violet, curcumin, donepezil, galantamine, memantine, methylene blue, oleocanthal, rivastigmine, carbidopa, levodopa, and bromoergocryptine associated with Alzheimer, Parkinson diseases and neuroprotective agents for molecular docking interaction studies with 6LU7 and 7NEH [35-46].

#### *2.3.2. Preparation of receptor.*

Here, 6LU7 and 7NEH were considered for coronavirus (wild type and mutant B 1.1.7 strain) receptors PDB id. The structure of 6LU7 was procured from a protein data bank in PDB format. The co-crystallized ligand and water molecules were removed completely before interaction. The energy minimization process was performed using the steepest decent method. Then, all the polar hydrogens and Gasteiger charges were added to the receptor using AUTODOCK Tools 1.5.6 [47].

#### *2.3.3. Preparation of ligands.*

All the structures were procured from the PubChem database and saved in PDB format. Then, all the polar hydrogens and Gasteiger charges were added to the ligands using AUTODOCK Tools 1.5.6 [48].

#### *2.3.4 Parameters associated with molecular docking studies.*

Molecular docking studies were performed using AUTODOCK Vina, MGLTools, and PyMol software. The grid measurement values of docking performance were as follows: 6LU7: center\_x = (-) 18.407, center\_y = 12.577, center\_z = 60.161. size\_x = 24, size\_y = 24, size\_z = 24, exhaustiveness = 8. GLU 166 was considered a flexible residue. 7NEH:: center\_x = 1.903, center\_y = 72.062, center\_z = 16.274. size\_x = 24, size\_y = 24, size\_z = 24, exhaustiveness = 8. ASN 343 was considered a flexible residue [49].

## **3. Results and Discussion**

After performing prolonged and tedious sequence-sequence matching analysis (BLAST technique) between all the aforementioned receptors related to neurological disorders and

6LU7 (wild-type strain of COVID main protease) (Figure 2) [50-52]. The outcomes showed that 2V17 (receptor belongs to tau protein and Alzheimer’s disease), 6DCA(antigen-binding fragment (Fab)/epitope complex structure related to Alzheimer’s disease), 6DCW (human anti-tau antibody CB Tau -27.1 Fab in complex related to Alzheimer’s disease), 5E2U (Tau AT8 FAB associated with aggregation of aggregates of paired helical filaments (PHF- Tau) and Alzheimer’s disease), 6VMS (dopaminergic D2 receptor associated with Parkinson disease) and 6E4Y (PCSK9 fab 6E2 associated with brain injury and connective tissue insulation) were observed with noticeable percent similarities of 34.48%, 34.48%, 42.11%, 47.64%, 52.4% and 52.4%, respectively (Table 1) [53,54].

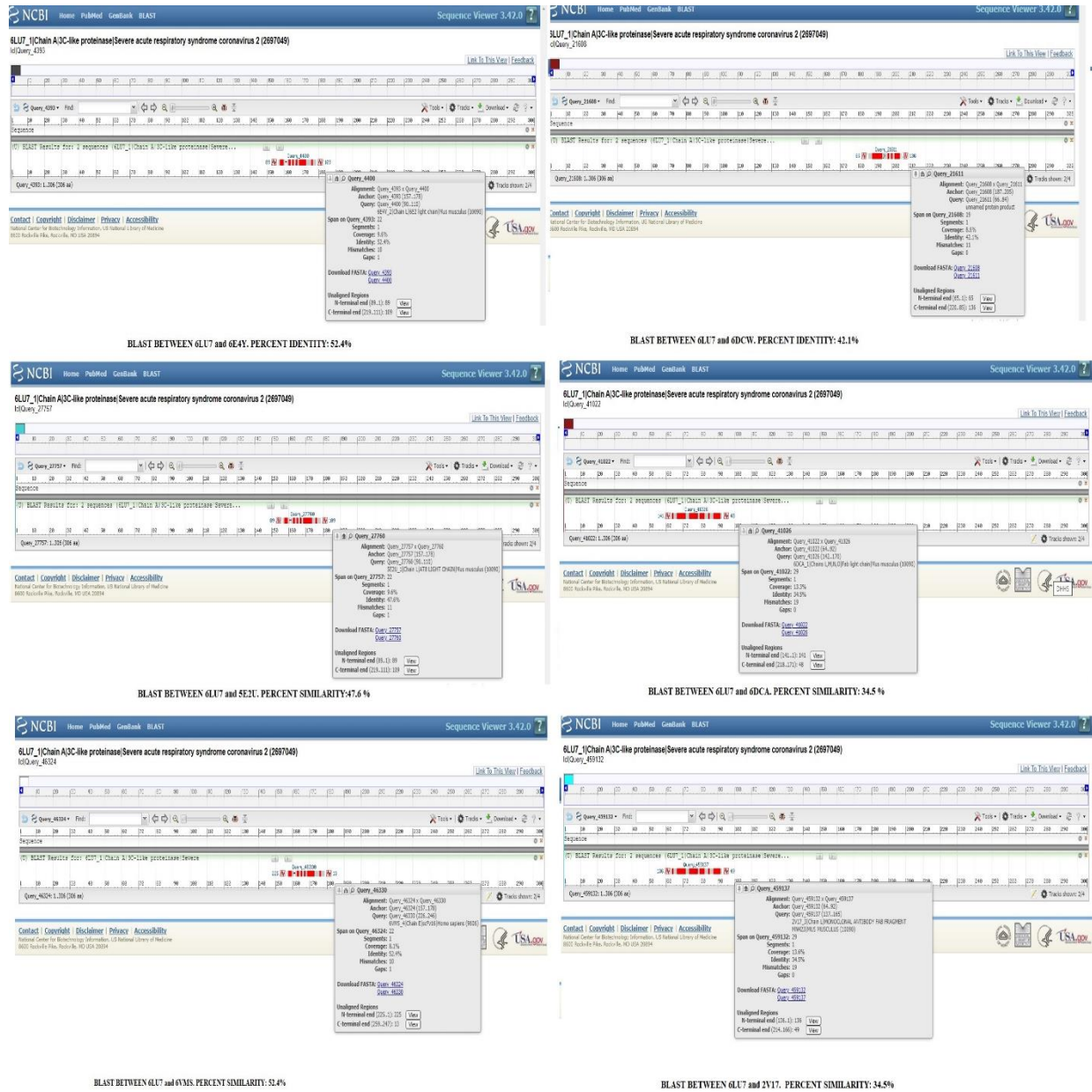


**Figure 2.** Protein-Protein sequence similarity data between 6LU7 with 2V17, 6DCA, 6DCW, 5E2U, 6E4Y, and 6VMS.

**Table 1.** Percent similarity between coronavirus and neurological disorders-related receptors.

Principle receptor related to coronavirus (PDB id)	Neurological disorders related receptors similar to coronavirus receptor	Percent similarity between the receptors
6LU7	2V17 (Structure of the complex of antibody MN423 with a fragment of tau protein)	34.48%

Principle receptor related to coronavirus (PDB id)	Neurological disorders related receptors similar to coronavirus receptor	Percent similarity between the receptors
(Crystal structure of COVID-19 main protease in complex with an inhibitor N3)	6DCA (Fab/epitope complex of mouse monoclonal antibody 6B2 targeting a non-phosphorylated tau epitope)	34.48%
	6DCW (Crystal structure of human anti-tau antibody CBTAU-27.1 Fab in complex with a human tau peptide)	42.11%
	5E2U (Structure of anti-TAU AT8 FAB in the presence of phosphopeptide)	47.64%
	6VMS (Structure of a D2 dopamine receptor-G-protein complex in a lipid membrane)	52.4%
	6E4Y (Anti-PCSK9 fab 6E2 bound to the N-terminal peptide from PCSK9)	52.4%

In the case of sequence-sequence matching analysis between all the aforementioned receptors related to neurological disorders and 7NEH (SARS-COV-2-B.1.17) (Figure 3). The outcomes showed that 2V17 (receptor belongs to tau protein and Alzheimer’s disease), 6DCA (antigen-binding fragment (Fab)/epitope complex structure related to Alzheimer’s disease), 6DCW (human anti-tau antibody CB Tau -27.1 Fab in complex related to Alzheimer’s disease), 5E2U (Tau AT8 FAB associated with aggregation of aggregates of paired helical filaments (PHF- Tau) and Alzheimer’s disease), 6VMS (dopaminergic D2 receptor associated with Parkinson disease) and 6E4Y (PCSK9 fab 6E2 associated with brain injury and connective tissue insulation) were observed with noticeable percent similarities of 63.96%, 52.27%, 73.78%, 72.40%, 67.8% and 78.22%, respectively (Table 2) [55-57].

**Table 2.** Percent similarity between coronavirus mutant strain B 1.1.7 and neurological disorders-related receptors.

Principle receptor related to coronavirus (PDB id)	Neurological disorders related receptors similar to coronavirus receptor	Percent similarity between the receptors
7NEH (Crystal structure of the receptor binding domain of SARS-CoV-2 Spike glycoprotein in complex with COVOX-269 Fab)	2V17 (Structure of the complex of antibody MN423 with a fragment of tau protein)	63.96%
	6DCA (Fab/epitope complex of mouse monoclonal antibody 6B2 targeting a non-phosphorylated tau epitope)	52.27%
	6DCW (Crystal structure of human anti-tau antibody CBTAU-27.1 Fab in complex with a human tau peptide)	73.78%
	5E2U (Structure of anti-TAU AT8 FAB in the presence of phosphopeptide)	72.40%
	6VMS (Structure of a D2 dopamine receptor-G-protein complex in a lipid membrane)	67.8%
	6E4Y (Anti-PCSK9 fab 6E2 bound to the N-terminal peptide from PCSK9)	78.22%

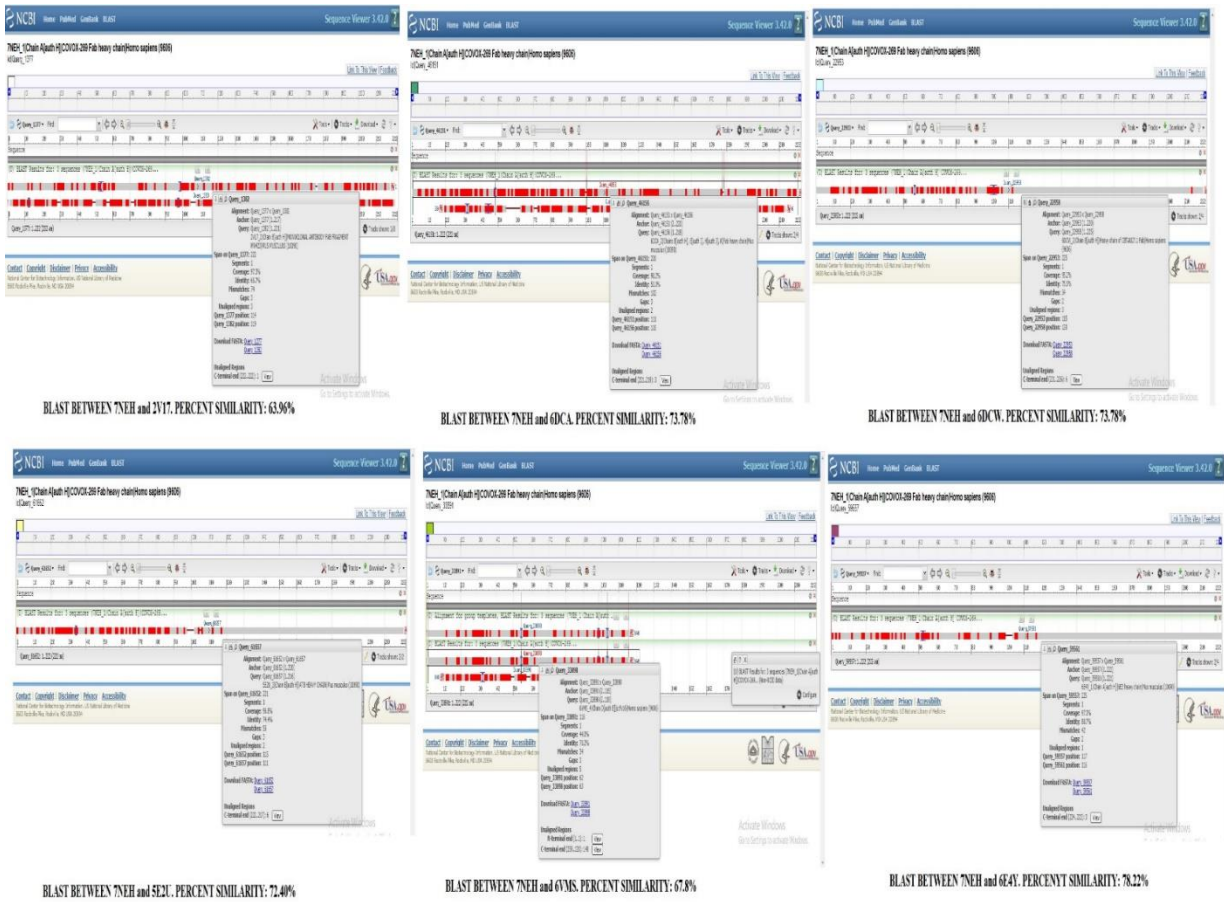


**Figure 3.** Protein-Protein sequence similarity data between 7NEH with 2V17, 6DCA, 6DCW, 5E2U, 6E4Y, and 6VMS.

These sequence similarity data revealed that if a patient suffered from any coronavirus infection (wild type or mutant), there was a chance for the occurrence of neurological disorders associated with PCSK9 fab 6E2 lead brain injury, and connective tissue insulation, tau protein accumulation related Alzheimer as well as abnormal dopaminergic D2 receptor linked Parkinson disease [58-60]. This information motivated us to go further to perform molecular docking interactions between selected neuroprotective agents (mainly used in the treatment of Alzheimer's, Parkinson's, brain ischemia [61,62], antiapoptotic behavior related to inhibition of caspase-3 enzyme, neuroprotection against age-induced neuronal apoptosis, autoimmune central nervous system inflammation) with 6LU7 and 7NEH [63,64]. The outcomes of molecular docking studies between selected neuroprotective agents and 6LU7 showed that binding energies lie between -10.2 Kcal/Mol and -4.3 Kcal/Mol (Table 3).

**Table 3.** Molecular docking interactions between selected neuroprotective agents and 6LU7.

Ligand Molecule	Receptor	Binding energy (Kcal/Mol)	RMSD values	Interactive residues present within 4.0 Å
Baicalein	6LU7	(-) 7.8	0.00	GLU 166 2.0 Å, HIS 163 2.5 Å, HIS 163 2.8 Å, SER 144 2.9 Å, SER 144 3.4 Å, SER 144 2.2 Å, LEU 141 3.1 Å, LEU 141 3.1, GLY 143 2.5 Å, CYS 145 3.0 Å
Baicalein quinone	6LU7	(-) 7.7	0.00	GLU 166 2.1 Å, HIS 163 2.3 Å, HIS 163 2.4 Å, SER 144 2.9 Å, SER 144 2.2 Å, SER 144 3.3 Å, LEU 141 3.1 Å, GLY 143 2.5 Å
Cinnamaldehyde	6LU7	(-) 4.3	0.00	CYS 145 3.2 Å, SER 144 3.1 Å, SER 144 2.2 Å, GLY 143 2.8 Å, LEU 141 2.9 Å

Ligand Molecule	Receptor	Binding energy (Kcal/Mol)	RMSD values	Interactive residues present within 4.0 Å
Crystal violet	6LU7	(-) 5.8	0.00	No interactive residues
Curcumin	6LU7	(-) 6.7	0.00	LEU 141 3.4 Å, THR 190 3.3 Å, GLU 166 2.6 Å
Donepazil	6LU7	(-) 7.7	0.00	No interactive residues
Galantamine	6LU7	(-) 7.3	0.00	GLY 143 2.5 Å, GLY 143 2.1 Å, HIS 163 2.2 Å
Memantine	6LU7	(-) 5.9	0.00	No interactive residues
Methylene blue	6LU7	(-) 6.3	0.00	No interactive residues
Oleocanthal	6LU7	(-) 6.6	0.00	HIS 164 3.4 Å, HIS 163 2.4 Å, HIS 41 2.8 Å
Rivastigmine	6LU7	(-) 5.6	0.00	GLY 143 2.4 Å, CYS 145 2.2 Å, SER 144 2.6 Å
Carbidopa	6LU7	(-) 5.8	0.00	GLN 189 3.3 Å, LEU 141 3.4 Å, ASN 142 3.6 Å, HIS 163 2.0 Å
Levodopa	6LU7	(-) 5.3	0.00	GLY 143 2.2 Å, GLY 143 2.6 Å, SER 144 2.1 Å, SER 144 3.2 Å, SER 144 2.9 Å
Bromoergocryptine	6LU7	(-) 10.2	0.00	HIS 172 2.2 Å, PRO 168 3.5 Å (π-π interaction)
AC-11	6LU7	(-) 5.6	0.00	No interactive residues
Acetyl-L-carnitine	6LU7	(-) 4.7	0.00	HIS 163 1.9 Å, CYS 145 2.3 Å, SER 144 2.2 Å
Acetylcysteine	6LU7	(-) 4.6	0.00	GLY 143 2.1 Å, GLY 143 2.7 Å, SER 144 2.1 Å, CYS 145 2.4 Å
Alpha-synuclein	6LU7	(-) 8.2	0.00	GLU 166 3.8 Å
Caffeine	6LU7	(-) 5.1	0.00	GLY 143 2.1 Å, LEU 141 3.3 Å
Citicoline	6LU7	(-) 7.6	0.00	GLN 189 3.4 Å, GLU 166 2.8 Å, HIS 163 2.2 Å, GLY 143 2.1 Å, SER 144 2.8 Å, LEU 141 3.0 Å, CYS 145 2.6 Å
Melatonin	6LU7	(-) 6.1	0.00	No interactive residues
Minocycline	6LU7	(-) 8.5	0.00	ASN 142 3.1 Å, LEU 141 3.2 Å, HIS 163 2.0 Å
Resveratrol	6LU7	(-) 6.3	0.00	GLU 166 2.2 Å, HIS 163 2.0 Å, SER 144 3.2 Å, LEU 141 3.2 Å
Selegiline	6LU7	(-) 5.0	0.00	No interactive residues
Sodium phenylbutyrate	6LU7	(-) 5.0	0.00	HIS 163 2.1 Å

In the case of 7NEH, binding energies lie between -8.4 Kcal/Mol and -4.3 Kcal/Mol (Table 4).

**Table 4.** Molecular docking interactions between selected neuroprotective agents and 7NEH.

Ligand Molecule	Receptor	Binding energy (Kcal/Mol)	RMSD values	Interactive residues present within 4.0 Å
Baicalein	7NEH	(-) 6.9	0.00	ARG 346 2.5 Å, ARG 346 2.3 Å, THR 345 3.0 Å.
Baicalein quinone	7NEH	(-) 6.7	0.00	ARG 346 2.4 Å, ARG 346 2.3 Å, THR 345 3.0 Å.
Cinnamaldehyde	7NEH	(-) 4.6	0.00	SER 514 2.9 Å, ARG 355 2.5 Å
Crystal violet	7NEH	(-) 5.3	0.00	No Interactive residues
Curcumin	7NEH	(-) 6.2	0.00	LYS 356 2.2 Å, GLU 340 3.2 Å, SER 399 3.1 Å, VAL 341 3.3 Å, THR 345 2.7 Å, THR 345 2.6 Å
Donepazil	7NEH	(-) 6.8	0.00	No Interactive residues
Galantamine	7NEH	(-) 6.4	0.00	ARG 346 2.7 Å, SER 399 2.6 Å
Memantine	7NEH	(-) 6.6	0.00	No Interactive residues
Methylene blue	7NEH	(-) 5.1	0.00	No Interactive residues
Oleocanthal	7NEH	(-) 6.1	0.00	THR 345 2.2 Å, THR 345 3.2 Å, ALA 397 3.0 Å, SER 399 3.2 Å

Ligand Molecule	Receptor	Binding energy (Kcal/Mol)	RMSD values	Interactive residues present within 4.0 Å
Rivastigmine	7NEH	(-) 4.9	0.00	SER 399 3.7 Å
Carbidopa	7NEH	(-) 5.8	0.00	VAL 341 3.5 Å, SER 399 3.4 Å, SER 399 2.7 Å, ALA 397 3.2 Å
Levodopa	7NEH	(-) 5.2	0.00	ARG 355 2.3 Å, ARG 355 2.0 Å, PHE 464 3.4 Å
Bromoergocryptine	7NEH	(-) 8.4	0.00	TYR 396 2.6 Å, TYR 396 2.7 Å
AC-11	7NEH	(-) 6.8	0.00	ARG 357 2.8 Å
Acetyl-L-carnitine	7NEH	(-) 4.5	0.00	ALA 248 2.1 Å
Acetylcysteine	7NEH	(-) 4.3	0.00	SER 399 2.1 Å, ALA 248 2.5 Å
Alpha-synuclein	7NEH	(-) 7.1	0.00	ASN 354 2.5 Å, ARG 355 2.2 Å
Caffeine	7NEH	(-) 4.9	0.00	SER 399 2.7 Å
Citicoline	7NEH	(-) 6.7	0.00	GLU 516 3.5 Å, GLU 516 3.6 Å, ARG 355 2.6 Å, ARG 355 2.2 Å, ARG 355 2.1 Å
Melatonin	7NEH	(-) 5.5	0.00	ASN 354 2.5 Å, SER 399 2.1 Å
Minocycline	7NEH	(-) 7.0	0.00	ARG 357 2.4 Å, TYR 396 3.2 Å, ASN 354 2.2 Å, ARG 357 2.0 Å
Resveratrol	7NEH	(-) 6.0	0.00	THR 345 2.1 Å, THR 345 2.1 Å, ALA 397 3.5 Å
Selegiline	7NEH	(-) 4.8	0.00	No interactive residues
Sodium phenylbutyrate	7NEH	(-) 5.3	0.00	ARG 355 2.3 Å

Here, we considered interaction within 4Å of the ligand molecule [65,66]. In the case of 6LU7, we found that crystal violet, donepezil, memantine, methylene blue, AC-11, melatonin, and selegiline were not interactive with any active site amino acids within the 4Å range. In the case of 7NEH, crystal violet, donepezil, memantine, methylene blue, and selegiline. In the case of 6LU7, the best four docking interactions observed with bromoergocryptine -10.2 Kcal/Mol, minocycline - 8.5 Kcal/Mol, alpha-synuclein - 8.2 Kcal/Mol and baicalein - 7.8 Kcal/Mol (Figure 4).

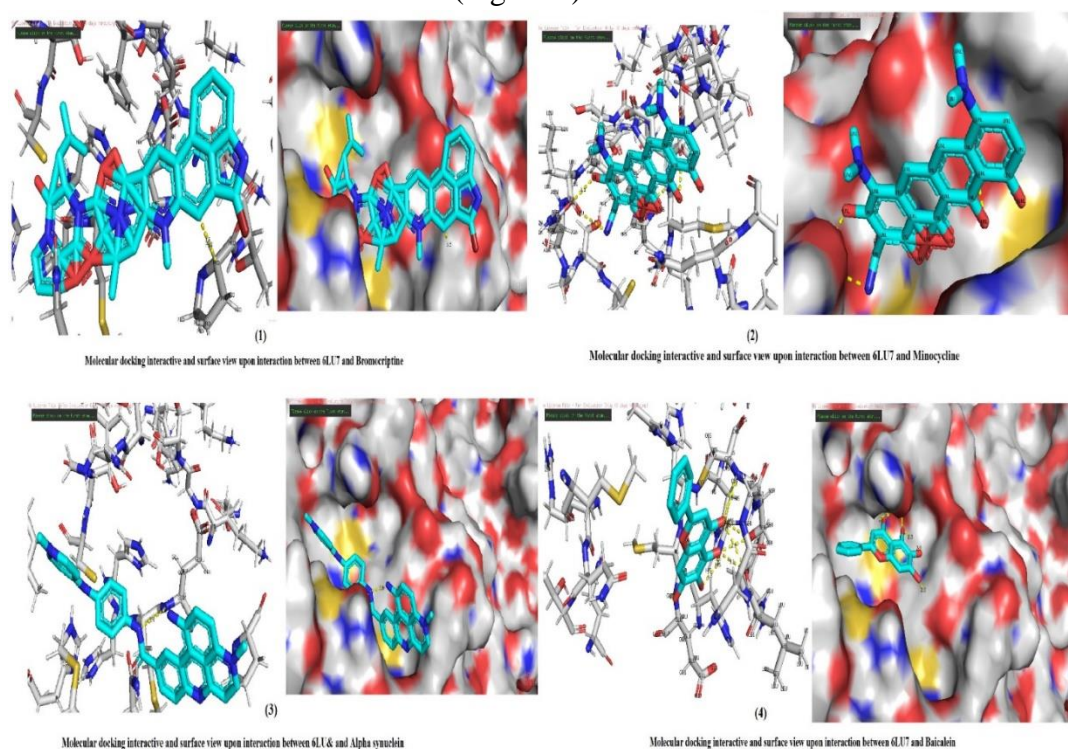


**Figure 4.** Molecular docking interaction data between selected neuroprotective agents and 6LU7.

The interactive residues of these ligands were HIS 172 2.2 Å, PRO 168 3.5 Å (Π-Π interaction) for bromoergocryptine, ASN 142 3.1 Å, LEU 141 3.2 Å, HIS 163 2.0 Å for minocycline, GLU 166 3.8 Å for alpha-synuclein and GLU 166 2.0 Å, HIS 163 2.5 Å, HIS 163 2.8 Å, SER 144 2.9 Å, SER 144 3.4 Å, SER 144 2.2 Å, LEU 141 3.1 Å, LEU 141 3.1, GLY 143 2.5 Å, CYS 145 3.0 Å for baicalein [67,68]. These data suggested that the aforementioned ligands were well docked within the receptor active site as surrounding residues of 6LU7 (active site) THR 190, GLU 166, GLN 189, ASP 187, HIS 164, PHE 140, CYS 145, GLY 143, HIS 172, SER 144, ASN 142, LEU 141, HIS 163, GLN 192 and MET 165 were similar with the interactive residues of bromoergocryptine, minocycline, alpha-synuclein and baicalein. In the case of 7NEH, the best four docking interactions observed with bromoergocryptine - 8.4 Kcal/Mol, alpha-synuclein - 7.1 Kcal/Mol, minocycline - 7.0 Kcal/Mol, and baicalein - 6.9 Kcal/Mol (Figure 5).

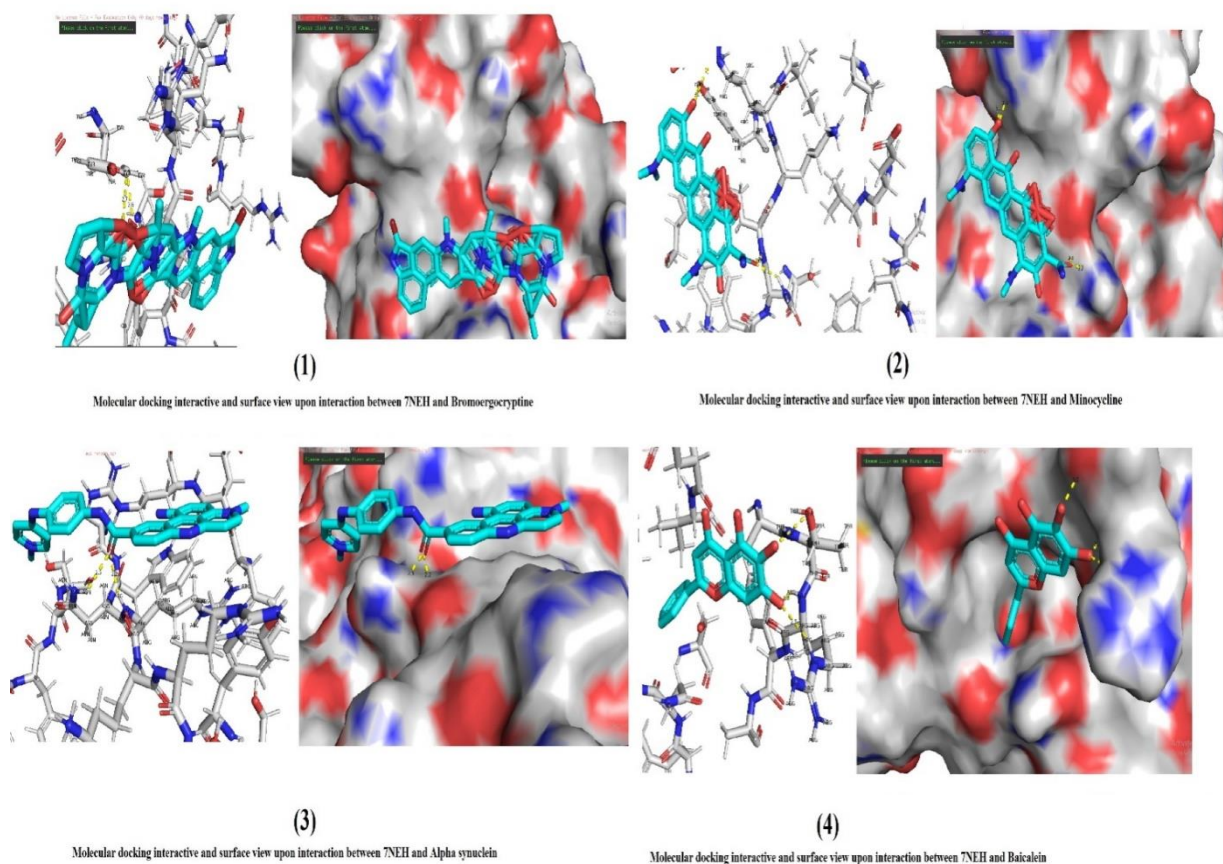


**Figure 5.** Molecular docking interaction data between selected neuroprotective agents and 7NEH.

The interactive residues of these ligands were TYR 396 2.6 Å, TYR 396 2.7 Å for bromoergocryptine, ASN 354 2.5 Å, ARG 355 2.2 Å for alpha-synuclein, ARG 357 2.4 Å, TYR 396 3.2 Å, ASN 354 2.2 Å, ARG 357 2.0 Å for minocycline and ARG 346 2.5 Å, ARG 346 2.3 Å, THR 345 3.0 Å for baicalein. These data suggested that aforementioned ligands were well docked within the receptor active site as surrounding residues of 7NEH (active site) ARG 346, THR 345, ARG 355, LYS 356 2.2 Å, GLU 340, SER 399, VAL 341, ALA 397, PHE 464 and ASN 354 were similar with the interactive residues of bromoergocryptine, alpha-synuclein, minocycline and baicalein [69,70]. Among all the neuroprotective agents that showed good receptor-ligand interaction, bromoergocryptine was observed to have the best interaction with both the receptors (6LU7 and 7NEH) and was fitted with a receptor active site.

## 4. Conclusion

The sequence similarity data suggested that if a person suffered from coronavirus infections, there was a probability for the development of neurological disorders associated with PCSK9 fab 6E2 lead brain injury and connective tissue insulation, tau protein accumulation related Alzheimer's as well as abnormal dopaminergic D2 receptor linked Parkinson disease. In conquering these conditions along with coronavirus infection, bromoergocryptine might be the best molecule. So, if we consider bromoergocryptine in for treating coronavirus infection, it may act as a good remedy for “Therapy of COVID-19” without any neurological disorder. Our data suggest and encourage further *in vitro* and *in vivo* investigations for repurposing neuroprotective agents therapeutically.

## Funding

Nil.

## Acknowledgment

Authors conveyed special thanks to Mr. Jitender Joshi, Chancellor, and Prof. (Dr.) Dharam Buddhi, Vice Chancellor of Uttaranchal University-Dehradun, encourages the publication of this research work. We are grateful to the Division of Research and Innovation (DRI) and Central Instrumentation Facility (CIF), Uttaranchal University-Dehradun, India, for providing all facilities during the experimental work.

## Conflict of Interests

Declared none.

## References

1. Marshall, M. How COVID-19 can damage the brain. *Nature* **2020**, 585, 342-343, <https://doi.org/10.1038/d41586-020-02599-5>.
2. Gralinski, L.E.; Menachery, V.D. Return of the Coronavirus: 2019-nCoV. *Viruses* **2020**, *12*, 135, <https://doi.org/10.3390/v12020135>.
3. UniProtKB. Available online: <https://www.uniprot.org/uniprot/?query=coronavirus&sort=score> (accessed on 16.09.2023).
4. Mao, L.; Jin, H.; Wang, M.; Hu, Y.; Chen, S.; He, Q.; Chang, J.; Hong, C.; Zhou, Y.; Wang, D.; Miao, X.; Li, Y.; Hu, B. Neurologic Manifestations of Hospitalized Patients With Coronavirus Disease 2019 in Wuhan, China. *JAMA Neurol.* **2020**, *77*, 683-690, <https://doi.org/10.1001/jamaneurol.2020.1127>.
6. Ftiha, F.; Shalom, M.; Jradeh, H. Neurological symptoms due to Coronavirus disease 2019. *Neurol. Int.* **2019**, *12*, 8639, <https://doi.org/10.4081/ni.2020.8639>.
7. Tripathi, N.; Tripathi, N.; Goshisht, M.K. COVID-19: inflammatory responses, structure-based drug design and potential therapeutics. *Mol. Divers* **2022**, *26*, 629-645, <https://doi.org/10.1007/s11030-020-10176-1>.
8. Berlit, P.; Bösel, J.; Gahn, G.; Isenmann, S.; Meuth, S.G.; Nolte, C.H.; Pawlitzki, M.; Rosenow, F.; Schoser, B.; Thomalla, G.; Hummel, T. “Neurological manifestations of COVID-19” - guideline of the German society of neurology. *Neurol. Res. Pract.* **2020**, *2*, 51, <https://doi.org/10.1186/s42466-020-00097-7>.
9. Altschul, S.F.; Gish, W.; Miller, W.; Myers, E.W.; Lipman, D.J. Basic local alignment search tool. *J. Mol. Biol.* **1990**, *215*, 403-410, [HTTPS://DOI.ORG/10.1016/S0022-2836\(05\)80360-2](https://doi.org/10.1016/S0022-2836(05)80360-2).
10. Jin, Z.; Du, X.; Xu, Y.; Deng, Y.; Liu, M.; Zhao, Y.; Zhang, B.; Li, X.; Zhang, L.; Peng, C.; Duan, Y.; Yu, J.; Wang, L.; Yang, K.; Liu, F.; Jiang, R.; Yang, X.; You, T.; Liu, X.; Yang, X.; Bai, F.; Liu, H.; Liu, X.; Guddat, L.W.; Xu, W.; Xiao, G.; Qin, C.; Shi, Z.; Jiang, H.; Rao, Z.; Yang, H. Structure of Mpro from SARS-CoV-2 and discovery of its inhibitors. *Nature* **2020**, 582, 289-293, <https://doi.org/10.1038/s41586-020-2223-y>.

11. Supasa, P.; Zhou, D.; Dejnirattisai, W.; Liu, C.; Mentzer, A.J.; Ginn, H.M.; Zhao, Y.; Duyvesteyn, H.M.E.; Nutalai, R.; Tuekprakhon, A.; Wang, B.; Paesen, G.C.; Slon-Campos, J.; López-Camacho, C.; Hallis, B.; Coombes, N.; Bewley, K.R.; Charlton, S.; Walter, T.S.; Barnes, E.; Dunachie, S.J.; Skelly, D.; Lumley, S.F.; Baker, N.; Shaik, I.; Humphries, H.E.; Godwin, K.; Gent, N.; Sienkiewicz, A.; Dold, C.; Levin, R.; Dong, T.; Pollard, A.J.; Knight, J.C.; Klennerman, P.; Crook, D.; Lambe, T.; Clutterbuck, E.; Bibi, S.; Flaxman, A.; Bittaye, M.; Belij-Rammerstorfer, S.; Gilbert, S.; Hall, D.R.; Williams, M.A.; Paterson, N.G.; James, W.; Carroll, M.W.; Fry, E.E.; Mongkolsapaya, J.; Ren, J.; Stuart, D.I.; Sreaton, G.R. Reduced neutralization of SARS-CoV-2 B.1.1.7 variant by convalescent and vaccine sera. *Cell* **2021**, *184*, 2201-2211.e2207, <https://doi.org/10.1016/j.cell.2021.02.033>.
12. Hubálek, F.; Binda, C.; Khalil, A.; Li, M.; Mattevi, A.; Castagnoli, N.; Edmondson, D.E. Demonstration of Isoleucine 199 as a Structural Determinant for the Selective Inhibition of Human Monoamine Oxidase B by Specific Reversible Inhibitors\*. *J. Biol. Chem.* **2005**, *280*, 15761-15766, <https://doi.org/10.1074/jbc.m500949200>.
13. Binda, C.; Li, M.; Hubálek, F.; Restelli, N.; Edmondson, D.E.; Mattevi, A. Insights into the mode of inhibition of human mitochondrial monoamine oxidase B from high-resolution crystal structures. *Proc. Natl. Acad. Sci. USA* **2003**, *100*, 9750-9755, <https://doi.org/10.1073/pnas.1633804100>.
14. De Colibus, L.; Li, M.; Binda, C.; Lustig, A.; Edmondson, D.E.; Mattevi, A. Three-dimensional structure of human monoamine oxidase A (MAO A): Relation to the structures of rat MAO A and human MAO B. *Proc. Natl. Acad. Sci. USA* **2005**, *102*, 12684-12689, <https://doi.org/10.1073/pnas.0505975102>.
15. Binda, C.; Aldeco, M.; Mattevi, A.; Edmondson, D.E. Interactions of Monoamine Oxidases with the Antiepileptic Drug Zonisamide: Specificity of Inhibition and Structure of the Human Monoamine Oxidase B Complex. *J. Med. Chem.* **2011**, *54*, 909-912, <https://doi.org/10.1021/jm101359c>.
16. Dowling, J.E.; Alimzhanov, M.; Bao, L.; Block, M.H.; Chuaqui, C.; Cooke, E.L.; Denz, C.R.; Hird, A.; Huang, S.; Larsen, N.A.; Peng, B.; Pontz, T.W.; Rivard-Costa, C.; Saeh, J.C.; Thakur, K.; Ye, Q.; Zhang, T.; Lyne, P.D. Structure and Property Based Design of Pyrazolo[1,5-a]pyrimidine Inhibitors of CK2 Kinase with Activity in Vivo. *ACS Med. Chem. Lett.* **2003**, *4*, 800-805, <https://doi.org/10.1021/ml400197u>.
17. Dowling, J.E.; Chuaqui, C.; Pontz, T.W.; Lyne, P.D.; Larsen, N.A.; Block, M.H.; Chen, H.; Su, N.; Wu, A.; Russell, D.; Pollard, H.; Lee, J.W.; Peng, B.; Thakur, K.; Ye, Q.; Zhang, T.; Brassil, P.; Racicot, V.; Bao, L.; Denz, C.R.; Cooke, E. Potent and Selective Inhibitors of CK2 Kinase Identified through Structure-Guided Hybridization. *ACS Med. Chem. Lett.* **2012**, *3*, 278-283, <https://doi.org/10.1021/ml200257n>.
18. Hackos, David H.; Lupardus, Patrick J.; Grand, T.; Chen, Y.; Wang, T.-M.; Reynen, P.; Gustafson, A.; Wallweber, Heidi J.A.; Volgraf, M.; Sellers, Benjamin D.; Schwarz, Jacob B.; Paoletti, P.; Sheng, M.; Zhou, Q.; Hanson, Jesse E. Positive Allosteric Modulators of GluN2A-Containing NMDARs with Distinct Modes of Action and Impacts on Circuit Function. *Neuron* **2016**, *89*, 983-999, <https://doi.org/10.1016/j.neuron.2016.01.016>.
19. Herguedas, B.; García-Nafría, J.; Cais, O.; Fernández-Leiro, R.; Krieger, J.; Ho, H.; Greger, I.H. Structure and organization of heteromeric AMPA-type glutamate receptors. *Science* **2016**, *352*, aad3873, <https://doi.org/10.1126/science.aad3873>.
20. Chen, S.; Zhao, Y.; Wang, Y.; Shekhar, M.; Tajkhorshid, E.; Gouaux, E. Activation and Desensitization Mechanism of AMPA Receptor-TARP Complex by Cryo-EM. *Cell* **2017**, *170*, 1234-1246.e1214, <https://doi.org/10.1016/j.cell.2017.07.045>.
21. Mathews, I.I.; Erion, M.D.; Ealick, S.E. Structure of Human Adenosine Kinase at 1.5 Å Resolution. *Biochemistry* **1998**, *37*, 15607-15620, <https://doi.org/10.1021/bi9815445>.
22. Sok, P.; Gógl, G.; Kumar, G.S.; Alexa, A.; Singh, N.; Kirsch, K.; Sebő, A.; Drahos, L.; Gáspári, Z.; Peti, W.; Reményi, A. MAP Kinase-Mediated Activation of RSK1 and MK2 Substrate Kinases. *Structure* **2020**, *28*, 1101-1113.e1105, <https://doi.org/10.1016/j.str.2020.06.007>.
23. Aoto, P.C.; Stanfield, R.L.; Wilson, I.A.; Dyson, H.J.; Wright, P.E. A Dynamic Switch in Inactive p38γ Leads to an Excited State on the Pathway to an Active Kinase. *Biochemistry* **2019**, *58*, 5160-5172, <https://doi.org/10.1021/acs.biochem.9b00932>.
24. Berg, S.; Bergh, M.; Hellberg, S.; Högdin, K.; Lo-Alfredsson, Y.; Söderman, P.; von Berg, S.; Weigelt, T.; Örmö, M.; Xue, Y.; Tucker, J.; Neelissen, J.; Jerning, E.; Nilsson, Y.; Bhat, R. Discovery of Novel Potent and Highly Selective Glycogen Synthase Kinase-3β (GSK3β) Inhibitors for Alzheimer's Disease: Design, Synthesis, and Characterization of Pyrazines. *J. Med. Chem.* **2012**, *55*, 9107-9119, <https://doi.org/10.1021/jm201724m>.

25. Meijer, L.; Skaltsounis, A.-L.; Magiatis, P.; Polychronopoulos, P.; Knockaert, M.; Leost, M.; Ryan, X.P.; Vonica, C.A.; Brivanlou, A.; Dajani, R.; Crovace, C.; Tarricone, C.; Musacchio, A.; Roe, S.M.; Pearl, L.; Greengard, P. GSK-3-Selective Inhibitors Derived from Tyrian Purple Indirubins. *Chem. Biol.* **2003**, *10*, 1255-1266, <https://doi.org/10.1016/J.CHEMBIOL.2003.11.010>.
26. Redenti, S.; Marcovich, I.; De Vita, T.; Pérez, C.; De Zorzi, R.; Demitri, N.; Perez, D.I.; Bottegoni, G.; Bisignano, P.; Bissaro, M.; Moro, S.; Martinez, A.; Storici, P.; Spalluto, G.; Cavalli, A.; Federico, S. A Triazolotriazine-Based Dual GSK-3 $\beta$ /CK-1 $\delta$  Ligand as a Potential Neuroprotective Agent Presenting Two Different Mechanisms of Enzymatic Inhibition. *Chem. Med. Chem.* **2019**, *14*, 310-314, <https://doi.org/10.1002/cmdc.201800778>.
27. Sevcik, J.; Skrabana, R.; Dvorsky, R.; Csokova, N.; Iqbal, K.; Novak, M. X-ray structure of the PHF core C-terminus: insight into the folding of the intrinsically disordered protein tau in Alzheimer's disease. *FEBS Lett.* **2007**, *581*, 5872-5878, <https://doi.org/10.1016/j.febslet.2007.11.067>.
28. Chukwu, J.E.; Congdon, E.E.; Sigurdsson, E.M.; Kong, X.-P. Structural characterization of monoclonal antibodies targeting C-terminal Ser<sup>404</sup> region of phosphorylated tau protein. *MAbs* **2019**, *11*, 477-488, <https://doi.org/10.1080/19420862.2019.1574530>.
29. Apetri, A.; Crespo, R.; Juraszek, J.; Pascual, G.; Janson, R.; Zhu, X.; Zhang, H.; Keogh, E.; Holland, T.; Wadia, J.; Verveen, H.; Siregar, B.; Mrosek, M.; Taggenbrock, R.; Ameijde, J.; Inganäs, H.; van Winsen, M.; Koldijk, M.H.; Zuijdgheest, D.; Borgers, M.; Dockx, K.; Stoop, E.J.M.; Yu, W.; Brinkman-van der Linden, E.C.; Ummenthum, K.; van Kolen, K.; Mercken, M.; Steinbacher, S.; de Marco, D.; Hoozemans, J.J.; Wilson, I.A.; Koudstaal, W.; Goudsmit, J. A common antigenic motif recognized by naturally occurring human VH5-51/VL4-1 anti-tau antibodies with distinct functionalities. *Acta Neuropathol. Commun.* **2018**, *6*, 43, <https://doi.org/10.1186/s40478-018-0543-z>.
30. Malia, T.J.; Teplyakov, A.; Ernst, R.; Wu, S.-J.; Lacy, E.R.; Liu, X.; Vandermeeren, M.; Mercken, M.; Luo, J.; Sweet, R.W.; Gilliland, G.L. Epitope mapping and structural basis for the recognition of phosphorylated tau by the anti-tau antibody AT8. *Proteins* **2016**, *84*, 427-434, <https://doi.org/10.1002/prot.24988>.
31. Yin, J.; Chen, K.-Y.M.; Clark, M.J.; Hijazi, M.; Kumari, P.; Bai, X.-c.; Sunahara, R.K.; Barth, P.; Rosenbaum, D.M. Structure of a D2 dopamine receptor-G-protein complex in a lipid membrane. *Nature* **2020**, *584*, 125-129, <https://doi.org/10.1038/s41586-020-2379-5>.
32. Ultsch, M.; Li, W.; Eigenbrot, C.; Di Lello, P.; Lipari, M.T.; Gerhardy, S.; AhYoung, A.P.; Quinn, J.; Franke, Y.; Chen, Y.; Kong Beltran, M.; Peterson, A.; Kirchhofer, D. Identification of a Helical Segment within the Intrinsically Disordered Region of the PCSK9 Prodomain. *J. Mol. Biol.* **2019**, *431*, 885-903, <https://doi.org/10.1016/j.jmb.2018.11.025>.
33. McCarthy, A.E.; Yoshioka, C.; Mansoor, S.E. Full-Length P2X<sub>7</sub> Structures Reveal How Palmitoylation Prevents Channel Desensitization. *Cell* **2019**, *179*, 659-670.e613, <https://doi.org/10.1016/j.cell.2019.09.017>.
34. Pearson, W.R. BLAST and FASTA Similarity Searching for Multiple Sequence Alignment. In *Multiple Sequence Alignment Methods*, Russell, D.J., Ed.; Humana Press, Totowa, NJ, **2014**; Volume 1079, 75-101, [https://doi.org/10.1007/978-1-62703-646-7\\_5](https://doi.org/10.1007/978-1-62703-646-7_5).
35. Ghai, R.; Nagarajan, K.; Arora, M.; Grover, P.; Ali, N.; Kapoor, G. Current Strategies and Novel Drug Approaches for Alzheimer Disease. *CNS Neurol. Disord. Drug Target.* **2020**, *19*, 676-690, <https://doi.org/10.2174/1871527319666200717091513>.
36. Shi, Z.; Lu, Z.; Zhao, Y.; Wang, Y.; Zhao-Wilson, X.; Guan, P.; Duan, X.; Chang, Y.-Z.; Zhao, B. Neuroprotective effects of aqueous extracts of *Uncaria tomentosa*: Insights from 6-OHDA induced cell damage and transgenic *Caenorhabditis elegans* model. *Neurochem. Int.* **2013**, *62*, 940-947, <https://doi.org/10.1016/j.neuint.2013.03.001>.
37. Zanelli, S.A.; Solenski, N.J.; Rosenthal, R.E.; Fiskum, G. Mechanisms of ischemic neuroprotection by acetyl-L-carnitine. *Ann. N. Y. Acad. Sci.* **2005**, *1053*, 153-161, <https://doi.org/10.1196/annals.1344.013>.
38. Berk, M.; Malhi, G.S.; Gray, L.J.; Dean, O.M. The promise of N-acetylcysteine in neuropsychiatry. *Trends Pharmacol. Sci.* **2013**, *34*, 167-177, <https://doi.org/10.1016/j.tips.2013.01.001>.
39. Ge, P.; Luo, Y.; Wang, H.; Ling, F. Anti-protein aggregation is a potential target for preventing delayed neuronal death after transient ischemia. *Med. Hypotheses* **2009**, *73*, 994-995, <https://doi.org/10.1016/j.mehy.2008.10.041>.
40. Ross, G.W.; Petrovitch, H. Current Evidence for Neuroprotective Effects of Nicotine and Caffeine Against Parkinson's Disease. *Drugs Aging* **2001**, *18*, 797-806, <https://doi.org/10.2165/00002512-200118110-00001>.

41. Li, W.; Lee, M.K. Antiapoptotic property of human  $\alpha$ -synuclein in neuronal cell lines is associated with the inhibition of caspase-3 but not caspase-9 activity. *J. Neurochem.* **2005**, *93*, 1542-1550, <https://doi.org/10.1111/j.1471-4159.2005.03146.x>.
42. Adibhatla, R.M.; Hatcher, J.F.; Dempsey, R.J. Citicoline: neuroprotective mechanisms in cerebral ischemia. *J Neurochem* **2002**, *80*, 12-23, <https://doi.org/10.1046/j.0022-3042.2001.00697.x>.
43. Tajés Orduña, M.; Pelegrí Gabalda, C.; Vilaplana Hortensi, J.; Pallàs Lliberia, M.; Camins Espuny, A. An evaluation of the neuroprotective effects of melatonin in an in vitro experimental model of age-induced neuronal apoptosis. *J. Pineal. Res.* **2009**, *46*, 262-267, <https://doi.org/10.1111/j.1600-079x.2008.00656.x>.
44. Maier, K.; Merkler, D.; Gerber, J.; Taheri, N.; Kuhnert, A.V.; Williams, S.K.; Neusch, C.; Bähr, M.; Diem, R. Multiple neuroprotective mechanisms of minocycline in autoimmune CNS inflammation. *Neurobiol. Dis.* **2007**, *25*, 514-525, <https://doi.org/10.1016/j.nbd.2006.10.022>.
45. Simão, F.; Matté, A.; Matté, C.; Soares, F.M.S.; Wyse, A.T.S.; Netto, C.A.; Salbego, C.G. Resveratrol prevents oxidative stress and inhibition of  $\text{Na}^+\text{K}^+$ -ATPase activity induced by transient global cerebral ischemia in rats. *J. Nutr. Biochem.* **2011**, *22*, 921-928, <https://doi.org/10.1016/j.jnutbio.2010.07.013>.
46. Ebadi, M.; Sharma, S.; Shavali, S.; El Refaey, H. Neuroprotective actions of selegiline. *J. Neurosci. Res.* **2002**, *67*, 285-289, <https://doi.org/10.1002/jnr.10148>.
47. Saha, S.; Pal, D.; Nimse, S.B. Recent Advances in the Discovery of GSK-3 Inhibitors from Synthetic Origin in the Treatment of Neurological Disorders. *Curr. Drug Targets* **2021**, *22*, 1437-1462, <https://doi.org/10.2174/1389450122666210120143953>.
48. Kaushik, B.; Pal, D.; Saha, S. Gamma Secretase Inhibitor: Therapeutic Target via NOTCH signaling in T Cell Acute Lymphoblastic Leukemia. *Curr. Drug Targets* **2021**, *22*, 1789-1798, <https://doi.org/10.2174/1389450122666210203192752>.
49. Pal, D.; Saha, S. Chondroitin: a natural biomarker with immense biomedical applications. *RSC Adv.* **2019**, *9*, 28061-28077, <https://doi.org/10.1039/c9ra05546k>.
50. Saha, S.; Banerjee, S.; Ganguly, S. Molecular Docking Studies of Some Novel Hydroxamic Acid Derivatives. *Int. J. ChemTech Res.* **2010**, *2*, 932-936.
51. Banerjee, S.; Saha, S.; Dawn, S. Design Strategy of Some Novel Tetrahydroquinoline Analogs as Potential Non-Nucleoside Reverse Transcriptase Inhibitors. *Der Pharm. Lett.* **2010**, *2*, 154-162.
52. Saha, S.; Acharya, M.; Prinsa. 2D QSAR Approach to Develop Newer Analogs as Melatonin Receptor Agonist. *Dhaka Univ. J. Pharm. Sci.* **2015**, *15*, 7-19.
53. Saha, S.; Pal, D.; Kumar, S. Design, synthesis and antiproliferative activity of hydroxyacetamide derivatives against HeLa cervical carcinoma cell and breast cancer cell line. *Tropical J. Pharm. Res.* **2016**, *15*, 1401-1411, <https://doi.org/10.4314/tjpr.v15i7.8>.
54. Chatterjee, D.; Maizel Jr., J.V. Sequence analysis of proteins. *Gene Anal. Tech.* **1987**, *4*, 27-40, [https://doi.org/10.1016/0735-0651\(87\)90015-x](https://doi.org/10.1016/0735-0651(87)90015-x).
55. Saha, S.; Jakhmola, V.; Mahato, A.K.; Ashok, P.K.; Warikoo, V.; Mukhopadhyay, S. QSAR model to develop newer generation GSK-3 $\beta$  inhibitors targeting Alzheimer. *Moroccan J. Chem.* **2023**, *11*, 897-1318, <https://doi.org/10.48317/IMIST.PRSM/morjchem-v11i04.39694>.
56. Saha, S.; Prinsa; Jakhmola, V.; Mahato, A.K.; Srivastava, S.; Dobhal, K.; Kawsar, S.M.A. *In Silico* Assessment of the Role of Iridoid in the Treatment of Zika and Influenza Virus Infection. *Philippine J. Sci.* **2023**, *152*, 1953-1988.
57. Kayes, M.R.; Saha, S.; Alanazi, M.M.; Ozeki, Y.; Pal, D.; Hadda, T.B.; Legssyer, A.; Kawsar, S.M.A. Macromolecules: Synthesis, antimicrobial, POM analysis and computational approaches of some glucoside derivatives bearing acyl moieties. *Saudi Pharm. J.* **2023**, *31*, 101804, <https://doi.org/10.1016/j.jsps.2023.101804>.
58. Kawsar, S.M.A.; Munia, N.S.; Saha, S.; Ozeki, Y. *In Silico* Pharmacokinetics, Molecular Docking and Molecular Dynamics Simulation Studies of Nucleoside Analogs for Drug Discovery- A Mini Review. *Mini Rev. Med. Chem.* **2024**, *24*, 1070-1088, <https://doi.org/10.2174/0113895575258033231024073521>.
59. Alamri, M.A.; Alawam, A.S.; Alshahrani, M.M.; Kawsar, S.M.A.; Prinsa; Saha, S. Establishing the Role of Iridoids as Potential Kirsten Rat Sarcoma Viral Oncogene Homolog G12C Inhibitors Using Molecular Docking; Molecular Docking Simulation; Molecular Mechanics Poisson–Boltzmann Surface Area; Frontier Molecular Orbital Theory; Molecular Electrostatic Potential; and Absorption, Distribution, Metabolism, Excretion, and Toxicity Analysis. *Molecules* **2023**, *28*, 5050, <https://doi.org/10.3390/molecules28135050>.

60. Almeahmadi, M.; Alsaiani, A.A.; Allahyani, M.; Alsharif, A.; Aljuaid, A.; Saha, S.; Asif, M. Computational studies and antimicrobial activity of 1-(benzo [d] oxazol-2-yl)-3, 5-diphenylformazan derivatives. *Curr. Comput.-Aided Drug Des.* **2024**, *20*, 835-846, <https://doi.org/10.2174/1573409919666230703103135>.
61. Almeahmadi, M.; Alsaiani, A.A.; Allahyani, M.; Aljuaid, A.; Saha, S.; Asif, M. Synthesis and *In Vitro* Antimycobacterial Activity of Some New *N*-(5-Substituted Phenylthiazol-2-yl) Pyrimidine-5-Carboxamides. *Indian J. Heterocycl. Chem.* **2023**, *33*, 221-226, <https://doi.org/10.59467/IJHC.2023.33.221>.
62. Fatonah, A.; Tambunan, U.S.F.; Pamungkas, W.O.; Dewanto, G.L.; Wicaksono, I.S. Discovery of GPX4 inhibitor by molecular docking simulation as a potential ferroptosis inducer. *Biointerface Res. Appl. Chem.* **2020**, *10*, 4929-4933, <https://doi.org/10.33263/BRIAC101.929933>.
63. Khaldan, A.; Bouamrane, S.; El-Mernissi, R.; Maghat, H.; Sbai, A.; Bouachrine, M.; Lakhliifi, T. Molecular docking, ADMET prediction, and quantum computational on 2-methoxy benzoyl hydrazone compounds as potential antileishmanial inhibitors. *Biointerface Res. Appl. Chem.* **2023**, *13*, 302, <https://doi.org/10.33263/BRIAC134.302>.
64. Obakiro, S.B.; K'Owino, I.; Kigundu, E.; Andima, M.; Owor, R.O.; Kiprop, A. Molecular Docking Interactions with Mycobacterial ATP and Polyketide-13 Synthase Enzymes of Phytoconstituents Isolated from *Entada abyssinica* Stem Bark. *Biointerface Res. Appl. Chem.* **2023**, *13*, 323, <https://doi.org/10.33263/BRIAC134.323>.
65. Akash, S.; Arefin, F.; Aovi, F.I. *In silico* Investigation of Potential Therapeutic Medication for the Inhibition of Dengue Virus (DENV NS2B/NS3 and NS1) by Modification of Polycyclic quaternary Alkaloid (Sanguinarine Derivatives) with Different Computational Approaches. *Biointerface Res. Appl. Chem.* **2023**, *13*, 403, <https://doi.org/10.33263/BRIAC135.403>.
66. Taidi, L.; Britel, M.R.; Amal, M. In silico study of selected lignins as COX-2 inhibitors. *Biointerface Res. Appl. Chem.* **2023**, *13*, 411, <https://doi.org/10.33263/BRIAC135.411>.
67. Hosseini, F.S.; Kazemzadeh, H.; Shahsavari, P.; Gholami, M.; Omrany, Z.B.; Amanlou, A.; Amanlou, M. Discovery of Novel Alanine Aminotransferase and Aspartate Aminotransferase Inhibitors by Large Scales Docking-Based Virtual Screening. *Biointerface Res. Appl. Chem.* **2023**, *13*, 412, <https://doi.org/10.33263/BRIAC135.412>.
68. Edache, E.I.; Uzairu, A.; Mamza, P.A.; Shallangwa, G.A. QSAR, homology modeling, and docking simulation on SARS-CoV-2 and pseudomonas aeruginosa inhibitors, ADMET, and molecular dynamic simulations to find a possible oral lead candidate. *J. Genet. Eng. Biotechnol.* **2022**, *20*, 88, <https://doi.org/10.1186/s43141-022-00362-z>.
69. Zaki, M.E.A.; Al-Hussain, S.A.; Masand, V.H.; Akasapu, S.; Bajaj, S.O.; El-Sayed, N.N.E.; Ghosh, A.; Lewaa, I. Identification of Anti-SARS-CoV-2 Compounds from Food Using QSAR-Based Virtual Screening, Molecular Docking, and Molecular Dynamics Simulation Analysis. *Pharmaceuticals* **2021**, *14*, 357, <https://doi.org/10.3390/ph14040357>.
70. Levine, K.S.; Leonard, H.L.; Blauwendraat, C.; Iwaki, H.; Johnson, N.; Bandres-Ciga, S.; Ferrucci, L.; Faghri, F.; Singleton, A.B.; Nalls, M.A. Virus exposure and neurodegenerative disease risk across national biobanks. *Neuron* **2023**, *111*, 1086-1093.e1082, <https://doi.org/10.1016/j.neuron.2022.12.029>.